ISSN 2321-807X

Ionic behavior, Na^+ mobility and infrared spectroscopy in $Na_7Cr_4(P_2O_7)_4PO_4$ material

Noura Fakhar Bourguiba[a,*], Habib Boughazala[a], Mohamed Faouzi Zid[a]

[a]Laboratoire de Matériaux et Cristallochimie, Faculté des Sciences, El Manar II, 2092 Tunis, Tunisia.

*Corresponding author. Tel: + 216 97 002 657

E-mail address: n.f.bourguiba@live.fr

Abstract

The title compound, heptasodium tetrachromium(III) tetrakis(diphosphate) orthophosphate, was synthesized by solid state reaction. Its structure is isotypic with that of $Na_7M_4(P_2O_7)_4PO_4$ (M = In, Al) compounds and is made up from a three-dimensional $[(CrP_2O_7)_4PO_4]^{7-}$ framework with channels running along [001]. The Na^+ cations are located in the voids of the framework. This compound has been investigated by X-ray diffraction and infrared (IR) spectroscopy. The conductivity measurements of the compound were carried out from 515 to 795 Kelvin using the frequency response analyzer with 0.05V amplitude signal over the range of 13MHz-5Hz. The conductivity of the sample at 574K is 0.45 10^{-6} $S.cm^{-1}$. The activation energy Ea=0.73eV shows that $Na_7Cr_4(P_2O_7)_4PO_4$ is a medium ionic conductors. The monovalent cations conduction pathways in the crystal bulks are simulated by means of the bond valence model (BVS).

Keywords: Three-dimensional structures; Tunnels; Rietveld; IR spectroscopy; Ionic Conductor; BVS.

Council for Innovative Research

Peer Review Research Publishing System

Journal: Journal of Advances in Chemistry

Vol. 10, No. 7

editorjaconline@gmail.com

www.cirjac.com

ISSN 2321-807X

1 Introduction

Materials with open-framework structures are of great importance in many fields of today's applied chemistry, such as ionic conductivity, ion-exchange, solid electrolytes for batteries, catalysis, positive electrode material [1-9]. The search for new phosphates and other materials with open-framework structures with increasing larger cavities has been extremely intensive in recent years.

In recent decades the exploration of A_2O-M_2O_3-P_2O_5 (A=monovalent cation and M=multivalent metal ion) system was used to isolate a large number of phosphates. Several well-known varieties of structures are reported in literature like NaSicon type $A_3M_2(PO_4)_3$ (A=monovalent ion, M = Al, Cr, Ti, Zr, Ga, Fe ...) [10-13], olivine structure $LiMPO_4$ (M=Fe, Al , Co.) [14,15]. The $Na_7M_4(P_2O_7)_4PO_4$ with (M = Fe, Al, Cr) compound family containing mono- and pyrophosphate groups was discovered by De la Rochère et al. [19]. In this series, the $Na_7In_4(P_2O_7)_4PO_4$ and $Na_7Al_4(P_2O_7)_4PO_4$ compounds were synthesized and investigated by Stus [20] et al. and Zhao [21] respectively. Using lithium, some other compounds like $Li_9V_3(P_2O_7)_3(PO_4)_2$ [16,17] and $Li_9M_3(P_2O_7)_3(PO_4)_2$ (M = Al, Ga, Cr, Fe) [18] were synthesized and structurally investigated.

We have recently reported the synthesis and crystal structure of $Na_7Cr_4(P_2O_7)_4PO_4$ [22]. The present paper is an extension of our work devoted to the preparation and characterization of $Na_7Cr_4(P_2O_7)_4PO_4$ compound by Rietveld method and Infrared spectroscopy. The ionic conductivity by complex impedance spectroscopy of this material is presented. A discussion over a correlation between structure and ionic conductivity is also reported.

2 Experimental section

A mixture of high purity reagents $NH_4H_2PO_4$ (Chareau, 62943), $NaHCO_3$ (Prolabo, 27778) and $CrCl_3.6H_2O$ (Merck, 2487), in stoichiometric ratios, is placed in the silica crucible. In order to eliminate volatile products, the sample is slowly annealed in air to 673 K for 24 h. In a second stage, several heat treatments in increments of 100K to 1023K with intermittent mixing and regrinding. The sample was slowly cooled at room temperature.

X-ray powder diffraction (XRPD) technique was used to identify and control the crystalline phase purity. XRPD pattern of powder sample was obtained on a D8 ADVANCE Bruker diffractometer with a Lynxeye accelerator using a Cu($K\alpha_1/\alpha_2$=1.54060/1.54439Å, $I\alpha_1/I\alpha_2$=2) wavelength.

The infrared absorption spectrum for $Na_7Cr_4(P_2O_7)_4PO_4$ was recorded at room temperature on a Nicolet IR200 FT-IR spectrometer, over range 1400-400 cm^{-1} using the KBr disk method.

Impedance spectroscopy measurements were carried out in a Hewlet-Packar 4192-A automatic bridge monitored by a HP microcomputer. Impedance spectra were recorded in the 13 MHz - 5 Hz frequency range with 0.5 V alternative signal. Pellet was prepared by uniaxial shaping followed by isostatic pressing at 2.5 kbar and sintering at 1073K for 2 h in air with 5 $K{\cdot}min^{-1}$ heating and cooling rates. The thickness and surface of pellet were about 1.44 mm and 0.74 cm^2 having a geometric factor of e/S = 0.195 cm^{-1}. Platinum electrodes were painted in the two faces of the pellet with a platinum paste to ensure good electric contacts and then painted pellet was carried out at steady-state temperatures in still air.

3 Results and discussion

3.1 X-Ray Diffraction

A single crystal X-ray diffraction was performed using an Enraf-Nonius CAD-4 diffractometer using the MoKα radiation at room temperature. The conditions for the collection of intensities, the experimental values and the refinement results are detailed in previous work [22]. The most important structural data are summarized in Table 1.

Table 1. Lattice parameters and reliability factors of $Na_7Cr_4(P_2O_7)_4PO_4$

Crystal system, Space group	**Tetragonal, P-42_1c**
Cell parameters (Å)	*a* = 14.058(2); *c* = 6.310(8)
Volume	1247.1 (3) $Å^3$
Reliability factors	$R[F^2 > 2\sigma(F^2)]$ = 0.023 ; $wR(F^2)$ = 0.064
Observed reflections	1277 $[I > 2\sigma(I)]$
Variable parameters	123

3.2 Structure description and discussion

The structure can be described as a three–dimensional framework of CrO_6 octahedra, PO_4 tetrahedra and P_2O_7 diphosphate groups linked by vertices. The Na^+ ions occupy interstitial sites (Fig. 1). The framework structural unit $[(CrP_2O_7)_4PO_4]^{7-}$, has the symmetry $\bar{4}$. It consists of a central tetrahedron PO_4 linked by each of its oxygens to a CrO_6

ISSN 2321-807X

octahedron; each octahedron is connected by two adjacent corners to a diphosphate group (P_2O_7). The $[(CrP_2O_7)_4PO_4]^{7-}$ units are stacked along the c axis to form columns. In the anionic framework each column binds to four neighbors by sharing vertices between polyhedra of different types to yield a three-dimensional structure exhibiting hexagonal tunnels running along c where the Na^+ cations are lodged.

The framework of the title compound is thus of open character and the motion of sodium cations through the tunnels seems feasible. This incites us to study the ionic conduction.

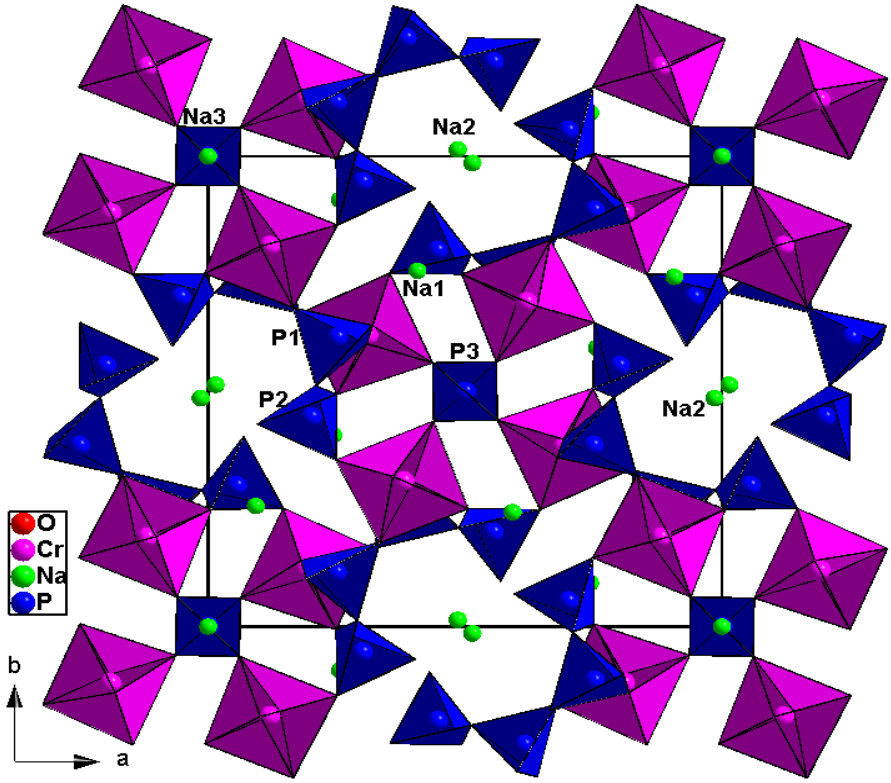

Fig 1: Projection of $Na_7Cr_4(P_2O_7)_4PO_4$ according to c showing channels where Na2 cations are located

3.3 Crystal morphology

The Bravais-Friedel-Donnay-Harker (BFDH) laws [23, 24] are strictly based on the symmetry of the crystal lattice to generate an ordered list of possible growing faces. The view of the observed and calculated crystal morphologies of $Na_7Cr_4(P_2O_7)_4PO_4$ reveals a similarity between the two shapes (see Figures 2 (a) and 2 (b)). This examination is used to assign the crystal growth axe as the (001), to identify the crystallographic axis and the physical ones.

ISSN 2321-807X

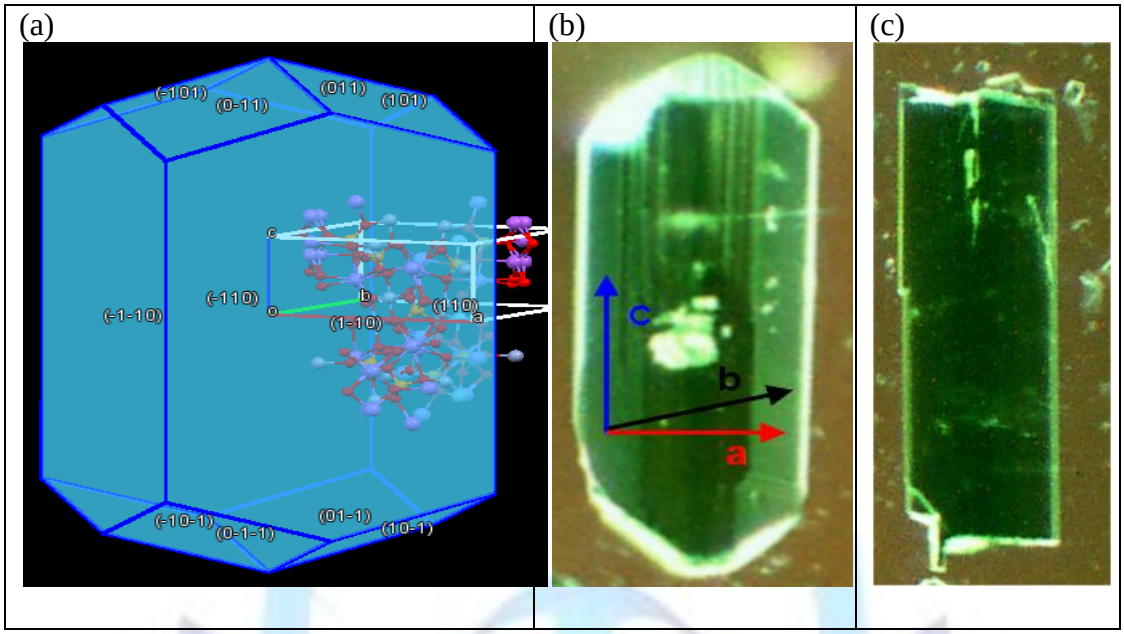

Fig 2: Growth shape from BFDH rules (a), the image of the growth morphologies is taken with the optical microscope of $Na_7Cr_4(P_2O_7)_4PO_4$ (b) and of $NaCrP_2O_7$ (c).

3.4 Infrared spectroscopy

Vibrations PO_4^{3-}

The internal vibrations consist predominantly of intramolecular stretching and bending motions of the PO_4^{3-} anions and are usually described in terms of the fundamental vibrations of the free anion (v1–v4). Bands between 650 and 400cm^{-1} are attributed to the harmonics of deformation of O–P–O angle (v2 and v4 modes) [25]. Bands in the region 580cm^{-1} are attributed to the asymmetric bending vibrational modes of O–P–O units [26]. The region 931–870cm^{-1} is assigned to PO_4^{3-} ionic group vibration [27].

Vibrations $P_2O_7^{4-}$

According to Corbridge [28], the assignment of the $P_2O_7^{4-}$ (or $O_3P–O–PO_3)^{4-}$ vibration modes is carried out in terms of PO_3 and P–O–P. The assignment of these different modes of vibration is based on a comparison of materials with related structures [29, 30]. In these conditions, the infrared bands for $Na_7Cr_4(P_2O_7)_4PO_4$ (Fig.3 and Table 2) are distributed in four distinct wavenumber ranges. The bands between 1180 and 1011 cm^{-1} are assigned to the stretching vibration modes of symmetrical and asymmetrical valence of P-O bond in the PO_3 and PO_4 groups. The absorption bands centered at 951 and 747 cm^{-1} are respectively associated to the asymmetric and symmetric modes of vibration of the P-O-P bridge in P_2O_7. The absorption bands between 673 and 518 cm^{-1} are attributed to the asymmetric deformation mode δas (O-P-O) PO_3 and PO_4. Symmetric modes of deformation δs (O-P-O) manifested themselves in the peaks centered at 448 and 413 cm^{-1}.

Table 2. Assignment of vibration frequencies in $Na_7Cr_4(P_2O_7)_4PO_4$ compound

Wave number (cm^{-1})	Assignment
1180, 1109	ν_{as}(P–O) dans PO_3 et PO_4
1048, 1011	ν_s(P–O) dans PO_3 et PO_4
951	ν_{as}(P–O–P) dans P_2O_7
747	ν_s(P–O–P) dans P_2O_7
673, 620, 590, 545, 518	δ_{as}(O–P–O) dans PO_3 et PO_4
448, 413	δ_s(O–P–O) dans PO_3 et PO_4

ISSN 2321-807X

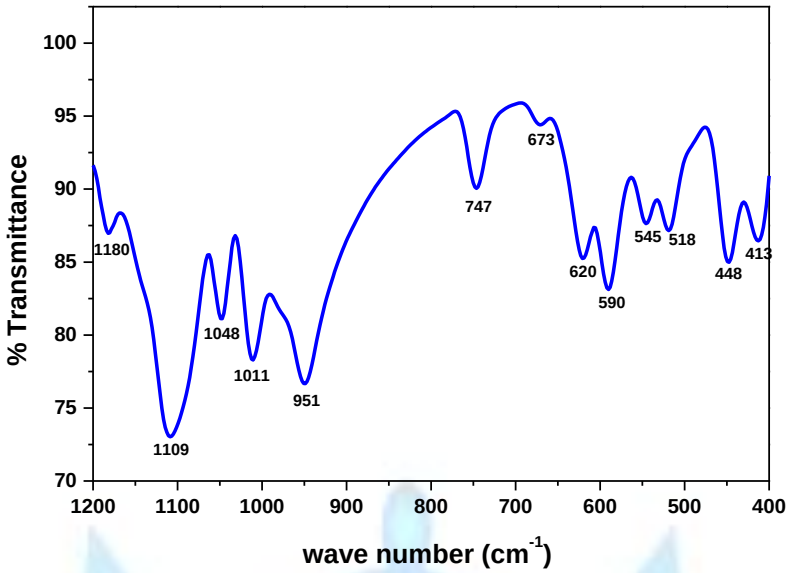

Fig 3: IR spectrum of $Na_7Cr_4(P_2O_7)_4PO_4$ compound

3.5 Rietveld refinement

About 1g of powder has been used for the diffraction experiment. Measurements were performed in spinning mode (60 tr.mn^{-1}), in order to minimize the preferential orientation effect of the crystallites, and a step-scanning ($\Delta 2\theta$=0.02°) at fixed time interval of 2s.

In the raw diffraction, the search-match procedure installed in the program EVA [32] and using the ICDD-PDF2 data base [33] allow the identification of $NaCrP_2O_7$ [34] in addition to $Na_7Cr_4(P_2O_7)_4PO_4$. Using the ICSD #31291 record for $NaCrP_2O_7$ and our recent structural investigation results [22] related to $Na_7Cr_4(P_2O_7)_4PO_4$, as basic structural models, the Rietveld refinements, carried out using the program TOPAS [31], allow a Quantitative Phase Analysis (QPA) and led to weight proportion of 90(1) % $Na_7Cr_4(P_2O_7)_4PO_4$ and 10(1)% $NaCrP_2O_7$. No structural information were refined except the parameters of the two cells.

The quantitative criteria of goodness of fits are the following agreement R factors:

$$R_P = \frac{\sum \left| Y_i.(obs) - \left(\frac{1}{c}\right) Y_i(cal) \right|}{\sum Y_i(obs)} \quad R_{\omega p} = \sqrt{\frac{\sum \omega_i \left[Y_i(obs) - \left(\frac{1}{c}\right) Y_i(calc) \right]^2}{\omega_i [Y_i(obs)]^2}} \quad GOF = \sqrt{\frac{\sum \omega_i \left[Y_i(obs) - \left(\frac{1}{c}\right) Y_i(calc) \right]^2}{N-p}}$$

where Y_i(obs) and Y_i(cal) are the observed and calculated intensities at the i^{th} step in the pattern, respectively. ω_i is the reciprocal of the variance of each observation, the summation is carried out over all the observations and 'c' is a scale factor.

Refinements results are summarized in Table 3 and Figure 4 shows the best agreement between observed and calculated profile with the difference curve corresponding to the last cycles of the refinement. The zoomed ranges 2θ (17-31)° (a) and (b) proof the presence of $NaCrP_2O_7$ in the mixture. Furthermore, the XRPD raw diffraction is marked with the presence of a large hump centred around 2θ=13°, signature of an amorphous part. The TOPAS degree of crystallinity calculation gives about 86% and can be explained by the incomplete chemical synthesis process.

ISSN 2321-807X

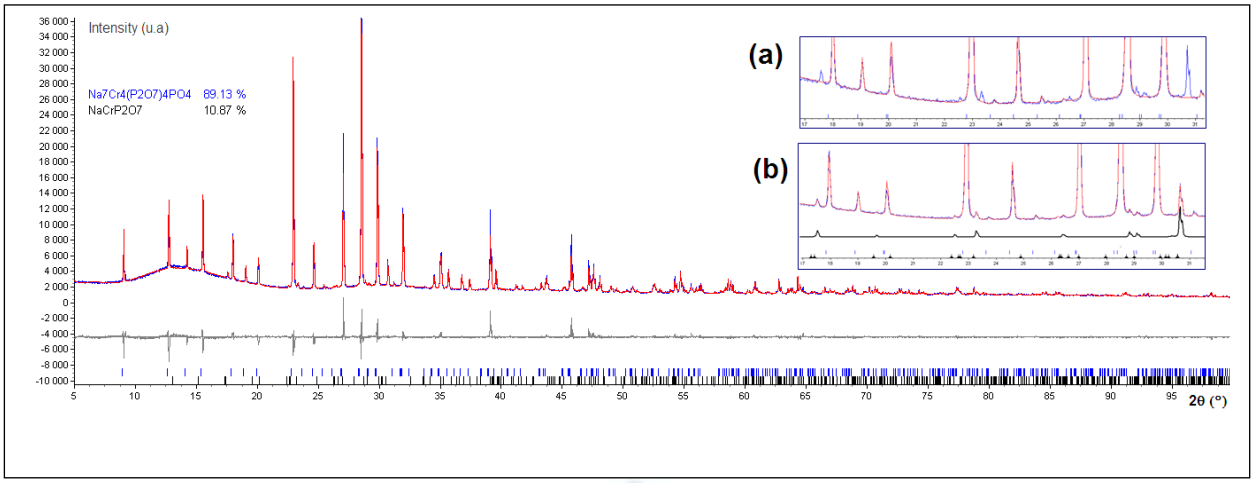

Fig 4 : The best agreement between observed and calculated profile with zooming range 2θ (17-31)° :

(a) Considering only $Na_7Cr_4(P_2O_7)_4PO_4$

(b) Considering both $Na_7Cr_4(P_2O_7)_4PO_4$ and $NaCrP_2O_7$

Table 3. Summary of the X-ray powder diffraction data measurements and the Rietveld refinements results

Data collection	Initial and refined cell parameters		Agreement factors and quantitative phase analysis
Radiation: Cu, λ Cu($K\alpha_1/\alpha_2$=1.54060/1.54439Å, $I\alpha_1/I\alpha_2$=2) Monochromator: graphite 2θ range: 5 – 100° Scan mode: θ -2θ Step width : 0.020° Time per step: 2.0s Power: I=40 mA U=40kV	Phase 1 Formula: $Na_7Cr_4(P_2O_7)_4PO_4$ S.G : P-42_1c a_s=14.058(2) c_s=6.3103(8) Refined cell parameters: a_p= 14.055(5)Å c_p= 6.309(2)Å	Phase 2 Formula: $NaCrP_2O_7$ S.G : $P2_1/c$ a_s=7.294(2) b_s=7.838(2) c_s=9.484(2) □$_s$=111.72(2) Refined cell parameters: a_p=7.285(8)Å b_p=7.826(9) Å c_p= 9.472(8)Å □$_p$=111.72(5)°	Background: Chebychev Profile function: pseudo-Voigt GOF: 2.55 R_{exp}: 2.33 R_{wp}: 5.70 R_p : 3.82 $Na_7Cr_4(P_2O_7)_4PO_4$ W_1= 90.0(1.0) % $NaCrP_2O_7$ W_2=10.0(1.0) %

3.6 Ionic transport behavior

Accordingly to the Rietveld refinement results previously presented, the ionic behavior discussed in this stage will be related to the main proportion in the analyzed powder ($Na_7Cr_4(P_2O_7)_4PO_4$ W_1=90.0%). Furthermore, to our knowledge, the second phase $NaCrP_2O_7$ is well-known by a low ionic conduction.

The Nyquist plots recorded for the bulk sample at various temperatures are shown in Figure 5. The electrical responses recorded at high frequency show two semicircle arcs which overlap and correspond to the migration of ions through the grains and grain boundaries. For each temperature the impedance diagram is fitted using ZView software [35]. The same equivalent circuit representing the two relaxations was used. The best fit is obtained when we used an equivalent circuit composed by the association in series of two cells each consisting of a resistor R connected in parallel with the impedance of CPE (constant-phase element). The CPE contribution is an empirical impedance function of the type:

$$Z(\omega)_{CPE} = 1/C(j\omega)^p ; \quad -1 \leq p \leq 1$$

ISSN 2321-807X

At each temperature the ohmic resistance is derived from complex impedance diagrams by the intersection of the extrapolation of the curve to higher frequencies with the real axis at zero phase angle. The fitted value of the resistance parameter of the sample at each temperature is presented in Table 4.

The conductivity value σ governed by the relationship is calculated from $\sigma=(e/s)/Z$ ($S.cm^{-1}$); e/s=g. Table 4 collects the conductivity values at different temperatures assigned probably to the $Na_7Cr_4(P_2O_7)_4PO_4$ material since it presents the main weight proportion of 90% in the analyzed sample (see 3.5. Rietveld refinement)

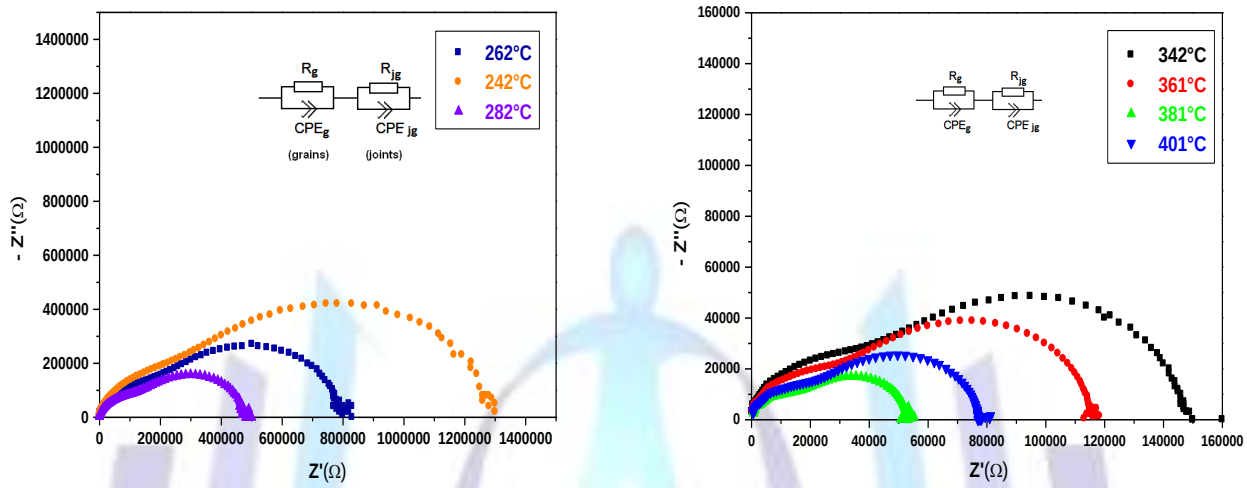

Fig 5: Impedance spectra recorded on $Na_7Cr_4(P_2O_7)_4PO_4$ sample at the temperature range 515-795K in air; the geometric factor g=0.195 cm^{-1}

Table 4. Values of fitted resistance (R), conductivity (σ) and Ln(σT) versus temperature for $Na_7Cr_4(P_2O_7)_4PO_4$ compound

T(K)	R(Ω)	σ($S.cm^{-1}$)	Ln(σT)
515	$1.200\ 10^{6}$	$1.503\ 10^{-7}$	-9.4684
535	$8.610\ 10^{5}$	$2.253\ 10^{-7}$	-9.0238
556	$4.958\ 10^{5}$	$3.912\ 10^{-7}$	-8.4356
564	$4.580\ 10^{5}$	$4.236\ 10^{-7}$	-8.3400
574	$4.360\ 10^{5}$	$4.449\ 10^{-7}$	-8.2742
615	$1.530\ 10^{5}$	$1.268\ 10^{-6}$	-7.1575
625	$1.380\ 10^{5}$	$1.406\ 10^{-6}$	-7.0411
634	$1.169\ 10^{5}$	$1.659\ 10^{-6}$	-6.8588
644	$1.000\ 10^{5}$	$1.940\ 10^{-6}$	-6.6846
654	$7.885\ 10^{4}$	$2.460\ 10^{-6}$	-6.4322
664	$6.736\ 10^{4}$	$2.879\ 10^{-6}$	-6.2596
674	$5.502\ 10^{4}$	$3.525\ 10^{-6}$	-6.0424
684	$4.035\ 10^{4}$	$4.807\ 10^{-6}$	-5.7065
694	$3.303\ 10^{4}$	$5.872\ 10^{-6}$	-5.5041
715	$2.112\ 10^{4}$	9.18310^{-6}	-5.0262
735	$1.589\ 10^{4}$	$1.220\ 10^{-5}$	-4.7142
754	$1.222\ 10^{4}$	$1.587\ 10^{-5}$	-4.4312
774	$0.992\ 10^{4}$	$1.955\ 10^{-5}$	-4.1930
795	$0.760\ 10^{4}$	$2.55\ 10^{-5}$	-3.8000

ISSN 2321-807X

The conductivity variation indicates an increasing with rise in temperature accordingly to the typical Arrhenius curve and traducing a linear dependence of thermal conductivity logarithm log(σT) versus $10^4/T$ (K^{-1}) (Fig. 6). This behavior indicates that the ionic conduction in the material is a thermally activated process and can follow $\sigma T=A^o \exp(-Ea/kT)$, where A^o is the pre-exponential factor, Ea the activation energy, T the absolute temperature and k the Boltzmann constant.

Obeying to the Arrhenius law, the obtained activation energy of $Na_7Cr_4(P_2O_7)_4PO_4$ sample is 0.73 eV. Thus, after rigorous measurements on the dense sample of $Na_7Cr_4(P_2O_7)_4PO_4$ material, the conductivity value at 574K is 0.45 10^{-6} $S.cm^{-1}$. Compared to the observed values in Table 5, the $Na_7Cr_4(P_2O_7)_4PO_4$ compound exhibits a mean ionic conductivity.

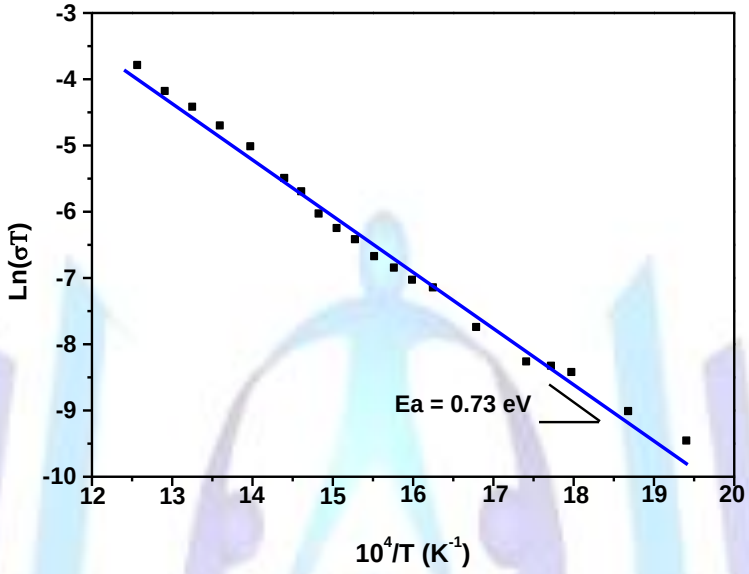

Fig 6: Arrhenius plots of conductivity of $Na_7Cr_4(P_2O_7)_4PO_4$ sample at the temperature range 515-795K

Table 5. Conductivity data of some materials in the literature

Material	T (K) range	E_a (eV)	σ ($\Omega^{-1}cm^{-1}$)	Ref
Low ionic conductors				
$K_3Cr_3(AsO_4)_4$	563-773	1.21	$\sigma_{703K} = 4.61\ 10^{-5}$	[47]
$AgCr_2(PO_4)(P_2O_7)$	661- 838	1.36	$\sigma_{750K} = 2.23\ 10^{-6}$	[30]
$(Na_{0,71}Ag_{0,29})_2CoP_2O_7$	573-773	1.368	$\sigma_{783K} = 1.2\ 10^{-6}$	[36]
Medium ionic conductors				
$K_3Cr_3(PO_4)_4$	693-769	0.9	$\sigma_{703K} = 5.16\ 10^{-6}$	[48]
$Na_4M_3(PO_4)_2(P_2O_7)$ (M = Mn, Co, Ni)	373-678	0.81-0.86	$\sigma_{573K(Ni)} = 2.1\ 10^{-6}$ $\sigma_{573K(Co)} = 1.3\ 10^{-6}$ $\sigma_{573K(Mn)} = 2.7\ 10^{-6}$	[37]
$Rb_3Sc_2(AsO_4)_3$	573-873	0.530	$\sigma_{750K} = 6.40\ 10^{-5}$	[38]
$Na_7Cr_4(P_2O_7)_4PO_4$	515-795	0.73	$\sigma_{574K} \approx 0.45\ 10^{-6}$	This work
$Na_7Fe_4(P_2O_7)_4PO_4$	523-723	0.71	$\sigma_{573K} = 1.6\ 10^{-6}$	[19]
Fast ionic conductors				
$Na_5YSi_4O_{12}$	308-403 403-623	0.2 0.3	$\sigma_{573K} = 3.0\ 10^{-2}$	[39]
$Na_5GdSi_4O_{12}$	308-403 403-623	0.23 0.31	$\sigma_{573K} = 2.80\ 10^{-2}$	[39]

ISSN 2321-807X

3.7 Conduction pathways proposed from bond valence analysis

The concept of Bond Valence Sum (BVS) [40,41] can be successfully used to simulate cations motion in the crystal bulk, such as lithium ion conduction in $La_{2/3-x}Li_{3x}TiO_3$ [42], sodium in NaSicon conductors [43], in $Na_2M_2(BO_3)_2O$ (M=Al, Ga) and $Na_{2-2x}Ca_xGa_2(BO_3)_2O$ (x=0.25; 0.50) [44] and silver in $Ag_3Nb(NbO)_2O_4(AsO_4)_2$ [45]. In this case, the BVS model offers a useful tool to relate the novel crystal structure to its ionic conductivity properties. Ionic pathways φ(x,y,z) are calculated from BVS in a large grid of points starting from initial crystallographic positions determined by X-ray diffraction. Analysing the φ(x,y,z) minima shows that low-activation energy motion occurs along particular migration directions such as tunnels connecting crystallographic sites or interlayer spaces. It has been shown that such procedure simulates the effect of external electrical force acting on the ion [46]. In the ionic pathways the lowest φ values correspond to stable positions, the highest values are associated to bottlenecks. The structural parameters resulting from X-ray analysis are assumed constant when the cations diffuse.

In the case of $Na_7Cr_4(P_2O_7)_4PO_4$ the Na2 motions appear to be able for migration along the *c*-axis (Fig.7(b)). The maximum φ(x,y,z) value for the sodium cations (called hereinafter Vumax) is φ(d)=1.27, the minimum is φ(d)=1.1 hopping distance more than 14Å. Furthermore, the Na1(Fig. 7(a)) ion appear to be ready for motion in the [101] and [011] directions with Vumax lower than 1.2 hopping distances up to 8 Å. The Na3 (Fig. 7(c)) ion motion seems difficult and the cations reach quickly bottlenecks Vumax exceeds 1.80 for short distances.

BVS analysis is in agreement with the suggestions derived from the structural study. Indeed, the most probable conduction paths are along [001] direction, in the hexagonal tunnels and the [101] direction. The hexagonal channels along [001] shown in Figure 8, are periodically delimited by two CrO_6 octahedra and six PO_4 tetrahedra. The shortest distance between two strangling oxygen on either side of the section pointing towards the center of the tunnel is around 3.33 Å. On the other hand, the largest distance (about 6.84Å) is more than twice the radii of the ions and thus more favorable to cationic displacement. The BVS modeling results can materialize the migration paths in the probable directions. These pathways are shown in Figure 9.

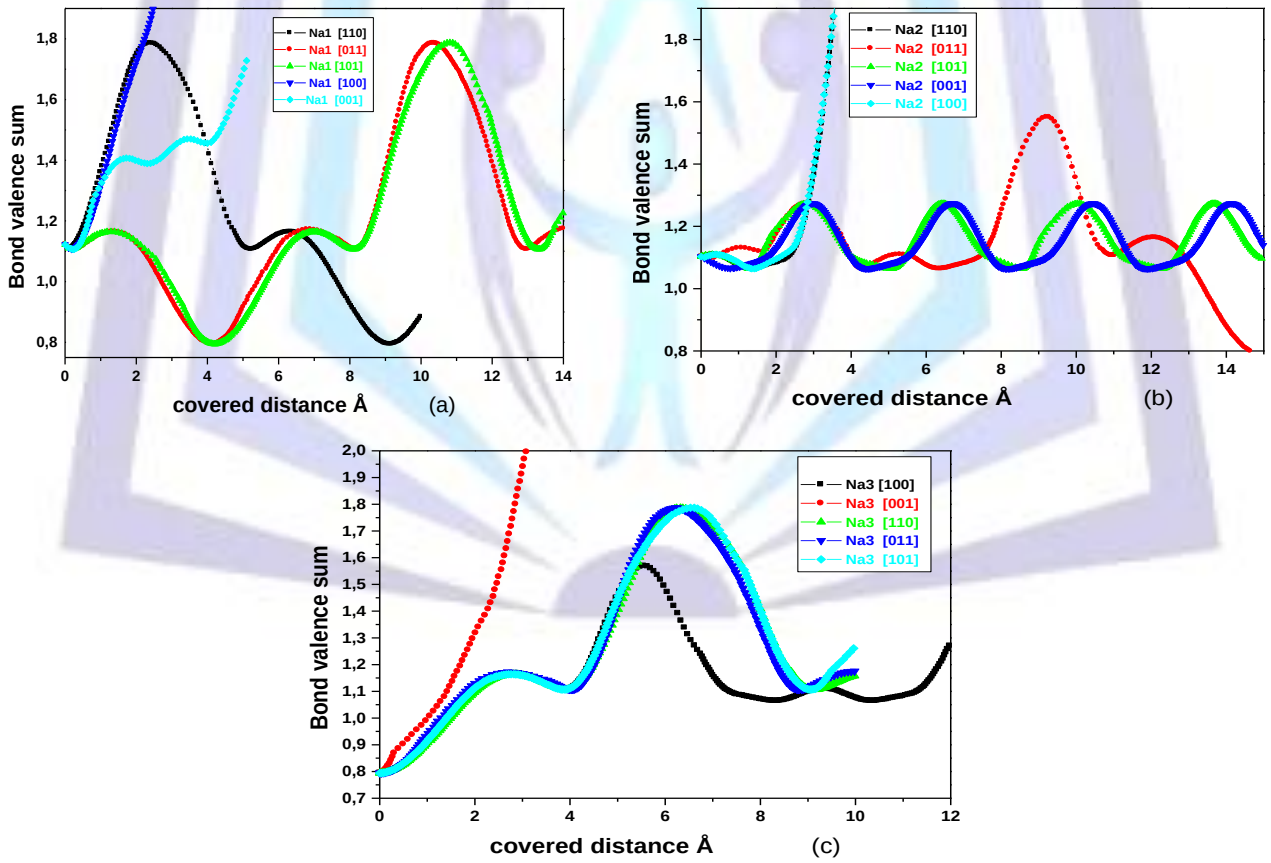

Fig 7: Bond valence sum for sodium ions: (a) Na1, (b) Na2, (c) Na3 vs the covered distance in $Na_7Cr_4(P_2O_7)_4PO_4$

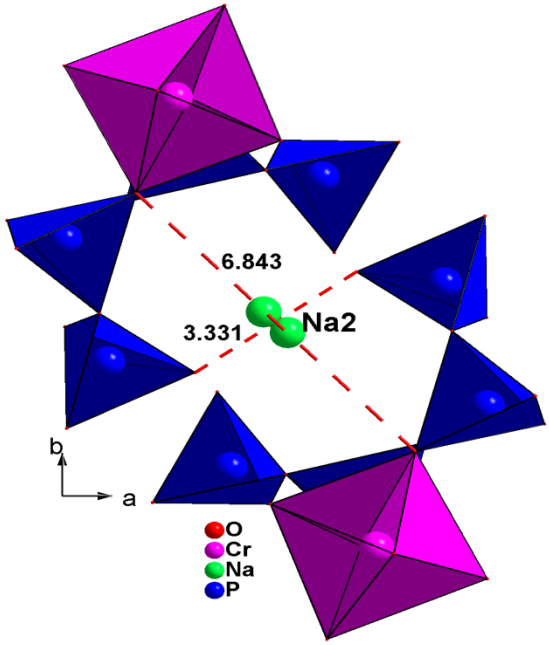

Fig 8: View of the shape and size of the [001] tunnel sections

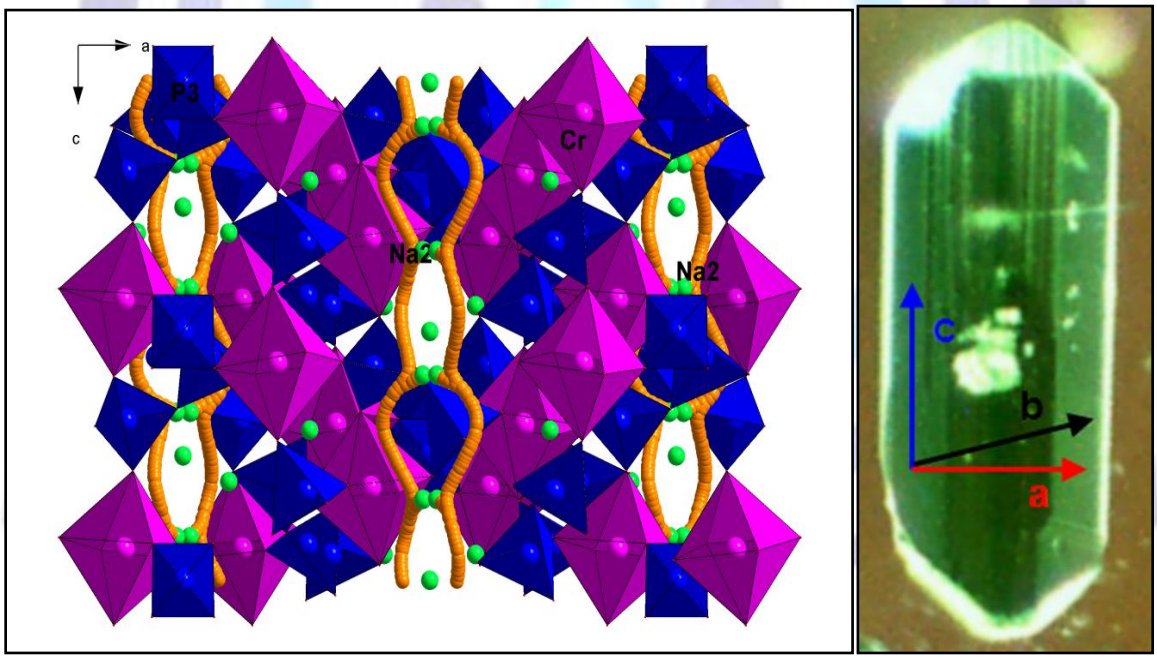

Fig 9: Schematic representation of the sodium conduction pathways along the [001] direction and its correspondence on the single crystal.

4 Conclusions

$Na_7Cr_4(P_2O_7)_4PO_4$ was synthesized by solid state reaction, characterized by single crystal X-ray diffraction and IR spectroscopy. The purity of the sample has been controlled by Rietveld powder diffraction technique. The structure contains tunnels along the [001] direction where the Na^+ ions are located. The open framework of the title compound and the location of the sodium ions make it a potential candidate for ionic conductivity. Ionic behaviors were investigated by complex impedance spectroscopy. The ionic conduction performances of the studied material led to 0.45 10^{-6} $S.cm^{-1}$

at 574K corresponding to an activation energy of 0.73eV. Therefore, compared to its homologous, it can be classified among the medium ionic conductors. The Bond Valence Sum (BVS) analysis was extended to modeling the ionic

conduction properties of alkali cations in the anionic framework. It shows that the conduction is better along the empty channels in the structure. A migration path according to these directions was modeled.

References

[1] H. Hong, Mater. Res. Bull., 11 (1976) 173–182.

[2] Ph. Colomban, Solid State Ionics, 21 (1986) 97–115.

[3] J. Alamo & R. Roy. J. Am. Ceram. Soc., 67 (1984) 78–80.

[4] C. Delmas, A. Nadiri, J.L. Soubeyroux, Solid State Ionics, 28–30 (1988) 419–423.

[5] M. Y. Saidi, J. Barker, H. Huang, J. L. Swoyer, G. Adamson, Electrochem. Solid State Lett. 5 (2002) A149.

[6] S. C. Yin, P. S. Strobel, H. Grondey, L. F. Nazar, Chem. Mater., 16 (2004) 1456–1465.

[7] M. Thomas, G. N. Greaves, G. Sankar, P. A. Wright, J. Chen, A. J. Dent, L. Marchese, Angew. Chem. Int. Ed.33 (1994) 1871-1873.

[8] O. Shigeto, S. Shoichiro, E. Minato, Y. Jun-ichi, J. Power Sources, 97–98 (2001) 430 – 432.

[9] A. Jain, G. Hautier, C. Moore, B. Kang, J. Lee, H. Chen, N. Twu, and G. Ceder, J. Electrochem. Soc., 159 (5) (2012) A622–A633.

[10] M. Catti, S. Stramare, Solid State Ionics, 136–137 (2000) 489–494.

[11] M. Barré, M. P. Crosnier-Lopez, F. Le Berre, E. Suard, J. L. Fourquet, J. Solid State Chem., 180 (3) (2007), 1011–1019.

[12] L. Vijayan, R. Cheruku, G. Govindaraj, S. Rajagopan, Mater. Chem. Phys., 130 (3) (2011) 862–869.

[13] Yu. Pinus, A. V. Khoroshilov, K. S. Gavrichev, V. P. Tarasov, A. B. Yaroslavtsev, Solid State Ionics, 212 (2012) 112-116.

[14] C. Chen, G.B. Liu, Y. Wang, J.L. Li, H. Liu, Electrochim. Acta, 113 (2013) 464–469.

[15] E. Markevich, R. Sharabi, O. Haik, V. Borgel, G. Salitra, D. Aurbach, G. Semrau, M.A. Schmidt, N. Schall, C. Stinner, J. Power Sources, 196 (15) (2011) 6433–6439.

[16] Z. Liang, Y. Zhao, Electrochim. Acta, 94 (2013) 374–380.

[17] Q. Kuang, J. Xu, Y. Zhao, X. Chen, L. Chen, Electrochim. Acta, 56, 5, (2011) 2201–2205.

[18] S. Poisson, F. d'Yvoire, NGuyen-Huy-Dung, E. Bretey, P. Berthet, J. Solid State Chem., 138 (1) (1998) 32–40

[19] M. De la Rochère, A. Khan, F. d'Yvoire, & E. Bretey, Mater. Res.Bull., 20 (1985) 27–34.

[20] N. V. Stus, V. V. Lisnyak, & P. G. Nagornyi, J. Alloys Compd., 314 (2001) 62–66.

[21] D. Zhao, Acta Cryst., E67 (2011) i64.

[22] N. Bourguiba Fakhar, M. F. Zid and A. Driss, Acta Cryst., E69 (2013) i27–i28.

[23] A. Bravais, *Etudes Crystallographiques*, Academie des Sciences,Paris, France, 2010.

[24] J. D. H. Donnay and D. Harker, "A new law of crystal morphology extending the Law of Bravais," *American Mineralogist*, vol. 22, p. 463, 1937.

[25] K. J. Rao, K. C. Sobha, S. Kumar, *Proc. Indian Acad. Sci.*, 113, (2001) 497–514.

[26] M. Sayer, A. Mansingh, Phys. Rev. B, 6 (1972) 4629–4643.

[27] A. Rulmont, R. Cahay, M. Liégeois-Duyckaerts, P. Tarte, Eur. J. Solid State Inorg. Chem., 28 (1991) 207–219.

[28] D.E. Corbridge, in: M. Grayson, G. Wiley (Eds.), Topics in Phosphorus Chemistry, Griffith Ed, New York, (1966), p. 275.

[29] A. Brahim, Comptes rendus Chimie,15 (2012) 603–608.

[30] R. Essehli, B. El Bali, S. Benmokhtar, H. Fuess, I. Svoboda, S. Obbade, J. Alloys Compd. 493 (2010) 654–660.

[31] Coelho, A. A. (2009). TOPAS, version 4.2 (Computer Software), Coelho Software, Brisbane.

[32] Bruker-AXS (2008). Diffracplus Evaluation package EVA 14, Release 15 (Computer Software) Bruker AXS GmbH Karlsruhe, Germany.

[33] ICDD (2010). Powder Diffraction File Inorganic and Organic Data Book, edited by Dr. Soorya Kabekkodu (International Centre for Diffraction Data, Newtown Square, PA USA), Set 60.

[34] L. Bohaty, J. Liebertz & R. Froehlich, Z. Kristallogr., 161(1982) 53-59

[35] Johnson, D. 1990—2007, Zview version 3.1c, Scibner Associates, Inc.

[36] M. Marzouki, A. Guesmi, M.F. Zid, A. Driss, Crystal Structure Theory and Applications, 1 (2012) 68–73.

[37] F. Sanz, C. Parada, J.M. Rojo and C. Ruíz-Valero, Chem. Mater., 13 (4) (2001) 1334–1340.

[38] J. M. Wimand, P. Tarte, C. R. Acad. Sci. Paris, Series II, 307 (1988) 1857–1862.

[39] N. Fakhar Bourguiba, N. Gharbi, L. Smiri Dogguy, J.P. Boilot, Mat. Res. Bull., 23 (1988) 1185–1191.

[40] I. D. Brown, "The Chemical Bond in Inorganic Chemistry - The Bond Valence Model," IUCr Monographs on Crystallography, 12, Oxford University Press, 2002.

[41] S. Adams, "Softbv", 2003. http://kristall.uni.mki.gwdg.de/softbv

[42] D. Mazza, S. Ronchetti, O. Bohnké, H. Duroy, J. L. Fourquet, Solid State Ionics, 149 (1-2) (2002) 81–88.

[43] D. Mazza, J. Solid State Chem., 156 (1) (2001) 154–160.

[44] G. Corbel, D. Mazza, O. Bohnké, M. Leblanc, Solid State Sciences, 7 (2005) 588–593.

[45] R. Ben Amor, A. Guesmi, D. Mazza, M. F. Zid, Journal de la Société Chimique de Tunisie, 10 (2008) 83–92.

[46] D. Mazza, J. Solid State Chem., 156 (2001) 154–160.

[47] B. Bouzemi, H. Boughzala and T. Jouini, J. Solid State Chem., 173, 273 (2003).

[48] S. Kouass and H. Boughzala, Phosphorus, Sulfur Silicon Relat. Elem., 181 (2006) 2641–2652.